JOURNAL OF GEOPHYSICAL RESEARCH, VOL. 104, NO. C4, PAGES 7683–7693, APRIL 15, 1999

Directional spreading of waves in the nearshore

T. H. C. Herbers
Department of Oceanography, Naval Postgraduate School, Monterey, California

Steve Elgar
School of Electrical Engineering and Computer Science, Washington State University, Pullman

R. T. Guza
Center for Coastal Studies, Scripps Institution of Oceanography, La Jolla, California

Abstract. Observations of surface gravity waves shoaling between 8-m water depth and the shoreline on a barred beach indicate that breaking results in an increase in the directional spread of wave energy, in contrast to the directional narrowing with decreasing depth predicted by refraction theory (Snell's law). During low-energy wave conditions, when breaking-induced wave energy losses over the instrumented transect are small, the observed mean propagation direction and spread about the mean both decrease with decreasing depth, consistent with the expected effects of refraction. Nonlinearity causes high-frequency components of the spectrum to become directionally aligned with the dominant incident waves. During high-energy wave conditions with significant wave breaking on the sand bar, the observed mean directions still decrease with decreasing depth. However, the observed directional spreads increase sharply (nominally a factor of 2 for values integrated over the swell-sea frequency range) between the outer edge of the surf zone and the crest of the sand bar, followed by a decrease toward the shoreline. Observations on a nonbarred beach also show directional broadening, with spreads increasing monotonically from the outer edge of the surf zone to a maximum value near the shoreline. Although the mechanism is not understood, these spatial patterns of directional broadening suggest that wave breaking causes significant scattering of incident wave energy into obliquely propagating components.

1. Introduction

The propagation directions of shoaling surface gravity waves change owing to refraction by spatial variations in water depth. If alongshore depth variations, currents, dissipation, and nonlinear effects are neglected, then both the wave frequency f and alongshore wavenumber l are conserved (Snell's law [e.g., *Kinsman*, 1965]). As the water depth h decreases, the wave incidence angle θ decreases, and in the shallow water limit

$$\theta = \frac{l}{2\pi f}(gh)^{1/2}. \tag{1}$$

where g is acceleration of gravity. Directional properties of shoaling waves are also affected by nonlinear energy exchanges between triads of wave components that obey the interaction rules [e.g., *Freilich et al.*, 1990; *Herbers and Burton*, 1997]:

$$f_1 + f_2 - f_3 = 0 \tag{2a}$$

$$l_1 + l_2 - l_3 = 0 \tag{2b}$$

In shallow water the sum interaction of two wave components (f_1, l_1) and (f_2, l_2) with small incidence angles θ_1 and θ_2 drives a higher-frequency ($f_3 = f_1 + f_2$, $l_3 = l_1 + l_2$) wave with a small angle θ_3 that is equal to the frequency-weighted average of θ_1 and θ_2 [equations (1) and (2)]:

$$\theta_3 = \frac{l_1 + l_2}{f_1 + f_2}\frac{(gh)^{1/2}}{2\pi} = \frac{f_1}{f_1 + f_2}\theta_1 + \frac{f_2}{f_1 + f_2}\theta_2 \tag{3}$$

Field [*Freilich et al.*, 1990] and laboratory [*Elgar et al.*, 1993] measurements confirm the effects of refraction [equation (1)] and nonlinear interactions [equation (3)] on nonbreaking shoaling waves.

Little is known about the effects of wave breaking on the directional properties of shoaling waves. Video observations show that incidence angles decrease as broken bore fronts approach the shoreline, qualitatively consistent with refraction [*Lippmann and Holman*, 1991]. However, initially straight wave crests sometimes appear to bend suddenly near locations separating breaking and nonbreaking portions of the wave crest. In a natural surf zone with irregular spatial fluctuations in wave-breaking patterns, these apparently random direction changes may cause a broadening of the directional distribution of wave energy, even on beaches with straight and parallel depth contours. Velocity measurements in the surf zone of a nearly plane beach indeed indicate a significantly stronger alongshore component of the wave orbital motion than is predicted by Snell's law [*Guza and Thornton*, 1985], consistent with a broadening of the directional spectrum. Analysis of array observations shows that a shore-parallel sand bar located within an energetic surf zone traps obliquely propagating waves in the incident swell frequency band [*Bryan and Bowen*, 1996]. However, the generation mechanism and importance of these bar-trapped edge waves are unknown.

In the present study the transformation of directional wave

Paper number 1998JC900092.
0148-0227/99/1998JC900092$09.00

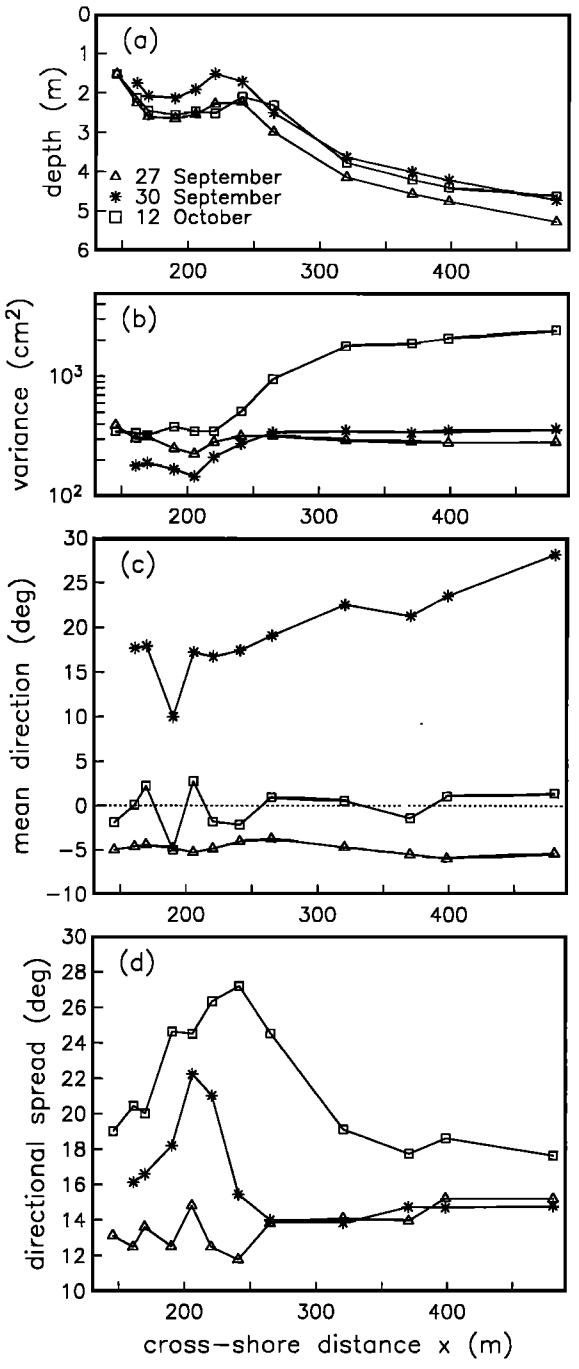

Figure 1. Three examples of the evolution of bulk-integrated (over swell-sea frequencies) directional wave properties observed along a cross-shore transect on a barred beach near Duck, North Carolina. (a) Water depth h. (b) Sea surface height variance. (c) Mean propagation direction θ_{mean}. (d) Directional spread σ_θ.

properties across a natural beach is investigated with field data from a dense cross-shore transect of collocated pressure sensors and current meters described in section 2. Although details of the directional wave spectrum are not resolved, a mean propagation direction θ_{mean} and a measure of the directional spreading of wave energy σ_θ can be estimated. Outside the surf zone the frequency-integrated (section 3) and frequency-dependent (section 4) estimates of θ_{mean} and σ_θ show the expected effects of refraction of incident waves toward normal incidence and the nonlinear excitation of similarly aligned [equation (3)] higher-frequency harmonics. Inside the surf zone, mean incidence angles remain small while directional spreads increase at all frequencies, suggesting that wave breaking causes directional scattering of wave energy. The role of the barred beach topography in the directional broadening of waves in the surf zone is discussed by comparison with observations from a nonbarred beach in section 5. The results are summarized in section 6.

2. Field Data

Wave measurements were collected during September and October 1994 on a sandy beach near Duck, North Carolina, that is exposed to swell arriving from the Atlantic Ocean. A collocated pressure transducer, bidirectional electromagnetic current meter, and sonar altimeter (to determine the seafloor location) were mounted approximately 50 cm above the seafloor at 14 positions along a 350-m-long cross-shore transect extending from near the shoreline (minimum depth about 1 m) to approximately 6 m depth (Figure 1a [*Elgar et al.*, 1997]). Incident wave properties were estimated from data obtained with a coherent array of 15 pressure gauges located in 8 m depth [*Long*, 1996], about 400 m directly offshore of the seaward end of the instrumented transect.

Pressure and velocity data were collected nearly continuously with a 2-Hz sample frequency. Spectra and cross-spectra were estimated at hourly intervals in the swell-sea frequency range of 0.05–0.25 Hz from 51.2-min-long data segments. A relatively wide frequency band width of 0.029 Hz was used to ensure stability (about 180 degrees of freedom) of directional moment estimates and to reduce variations in spectral levels resulting from phase coupling between incident and reflected wave components. Surface elevation spectra $E(f)$ were estimated from the pressure spectra using linear theory to account for attenuation over the water column. The data collection period includes several storms separated by calm periods. At the offshore array, significant wave heights ranged from 0.2 to 4 m and mean wave directions varied between −40° and 50°.

The beach profile is characterized by a shore-parallel sand bar that is submerged about 1.5–2.5 m below the mean sea surface (Figure 1a). The bottom slope is approximately 1:100 seaward of the sand bar. Shoreward of the sand bar, the depth increases by about 0.5 m into a relatively flat trough that extends to a steep (1:10) beach face. The crest of the sand bar was located about 120–150 m seaward of the shoreline during the first 45 days of these observations (e.g., cross-shore location 220–250 m in Figure 1a) and then migrated about 50 m farther offshore during a storm in mid-October [*Gallagher et al.*, 1998].

3. Directional Properties

A mean propagation direction θ_{mean} and a measure of the directional spreading of wave energy σ_θ (both functions of frequency) can be defined in terms of low-order Fourier moments of the frequency-directional wave spectrum $E(f, \theta)$ [equations (A3a) and (A3b)] [see also *Kuik et al.*, 1988, and references therein]:

$$\tan [2\theta_{\text{mean}}(f)] \equiv \frac{\int_{-\pi}^{\pi} d\theta \sin 2\theta E(f, \theta)}{\int_{-\pi}^{\pi} d\theta \cos 2\theta E(f, \theta)} \quad (4a)$$

$$\sigma_\theta^2(f) \equiv \frac{\int_{-\pi}^{\pi} d\theta \sin^2 [\theta - \theta_{\text{mean}}(f)] E(f, \theta)}{E(f)} \quad (4b)$$

These parameters can be estimated from the autospectra (C_{uu}, C_{vv}) and cospectrum (C_{uv}) of the horizontal velocity components u and v [see (A1c) and (A1d)] and have a simple physical interpretation. The mean angle θ_{mean}, where

$$\tan [2\theta_{\text{mean}}(f)] = \frac{2C_{uv}(f)}{C_{uu}(f) - C_{vv}(f)}, \quad (5)$$

represents the orientation (relative to shore normal) of the major principal axis of the fluctuating velocity vector (u, v) [e.g., *Higgins et al.*, 1981]. The polarization of the velocity field is given by the corresponding directional spread variable σ_θ:

$$\sigma_\theta^2(f) = \frac{C_{v'v'}(f)}{C_{u'u'}(f) + C_{v'v'}(f)} \quad (6)$$

where u', v' are the velocity components rotated into the principal axes coordinate frame [e.g., *Battjes*, 1972]. For directionally narrow wave fields ($C_{v'v'} \ll C_{u'u'}$), σ_θ is small and approximately equal to the half width of the directional distribution of wave energy (see appendix). For directionally broad wave fields, σ_θ is generally smaller than the directional half width, with a maximum value of $2^{-1/2}$ rad (or 40.5°) for an isotropic directional spectrum [equation (6) and Figure A1]. Note that θ_{mean} and σ_θ describe the directionality of the flow field without assuming linear wave motion and thus can be used to characterize directional wave properties both inside and outside the surf zone. Equations (5) and (6) were used to estimate $\theta_{\text{mean}}(f)$ and $\sigma_\theta(f)$ at all current meter locations. Estimates farther offshore in 8 m depth were obtained from the pressure array measurements using a different technique [*Elgar et al.*, 1994, Appendix A].

The largest source of error in the current meter estimates of θ_{mean} is uncertainty in the probe orientation relative to the beach. Estimates of this bias were obtained by comparing the current meter estimates of θ_{mean} at a frequency of 0.1 Hz (a band that is usually dominated by incident swell) with predictions obtained by transforming the 8-m depth pressure array estimates of θ_{mean} with Snell's law to all current meter locations. The differences between the current meter estimates and the predictions averaged over several-week periods (when the current meters were in a fixed position) indicate that rotation biases of the different current meters are randomly scattered between ±10°. All results presented here incorporate bias corrections based on these averaged differences. Subsequent observations with accurately oriented current meters (to be discussed elsewhere) confirm the validity of this procedure, and in any event the biases are small compared with the large range of observed wave directions. Current meter orientation errors do not affect estimates of the directional spread σ_θ.

Variations of bulk directional wave properties in the swell-sea frequency range are examined here with energy-weighted averages of the mean propagation direction θ_{mean} (4a) and directional spread σ_θ (4b)

$$\tan [2\theta_{\text{mean}}] \equiv \frac{\int_{0.05\text{Hz}}^{0.25\text{Hz}} df \int_{-\pi}^{\pi} d\theta \sin 2\theta E(f, \theta)}{\int_{0.05\text{Hz}}^{0.25\text{Hz}} df \int_{-\pi}^{\pi} d\theta \cos 2\theta E(f, \theta)} \quad (7a)$$

$$\sigma_\theta^2 \equiv \frac{\int_{0.05\text{Hz}}^{0.25\text{Hz}} df \int_{-\pi}^{\pi} d\theta \sin^2 (\theta - \theta_{\text{mean}}) E(f, \theta)}{\int_{0.05\text{Hz}}^{0.25\text{Hz}} df E(f)} \quad (7b)$$

Three representative examples of the cross-shore evolution of θ_{mean} and σ_θ are shown in Figures 1c and 1d, respectively. The beach profiles in these cases were similar with a well-developed sand bar at $x \approx 250$ m (Figure 1a). On September 27, low-amplitude incident waves (significant height in 8-m depth H_s = 0.7 m) resulted in nearly constant wave energy across the instrumented transect (Figure 1b) and a narrow surf zone confined to the steep beach face shoreward of the shallowest instrument. Along the entire transect, θ_{mean} is close to normal incidence (Figure 1c). The spreads σ_θ are also small, decreasing slightly (from 16° to 12°) toward the shore (Figure 1d). On September 30 at a lower tide stage (Figure 1a), waves with approximately the same offshore variance broke on the bar crest and were attenuated significantly at the shoreward end of the transect (Figure 1b). The mean direction decreases owing to refraction from 27° at the most offshore sensor to 16° on the bar crest and is approximately constant in the surf zone. The corresponding σ_θ decreases slightly from 16° to 14° between x = 480 and 250 m, followed by a sharp increase over the bar crest to a maximum value of 22° at x = 220 m and a decrease to 16° at x = 160 m. Dramatic directional broadening of waves in the surf zone was also observed on October 12 with more energetic (H_s = 2 m), nearly normally incident waves. While θ_{mean} is within 5° of normal incidence along the entire transect, σ_θ increases from 18° at the outer edge of the surf zone to a maximum value of 27° on the bar crest, decreasing again to 18° at the shoreward end of the transect.

The correspondence between surf zone wave breaking and directional broadening is demonstrated in Figure 2 by comparing the observed bulk directional spread with the bulk cross-shore energy flux at four cross-shore locations. The energy flux F_x

$$F_x = \rho g \int_{0.05\text{Hz}}^{0.25\text{Hz}} df c_g(f) \int_{-\pi}^{\pi} d\theta \cos \theta E(f, \theta) \quad (8)$$

where ρ is the density of seawater, g is the acceleration of gravity, and c_g is the group velocity, was estimated from pressure sensor–current meter cospectra with (A1a) and from the offshore pressure array data following *Elgar et al.* [1994]. The flux $\hat{F}_x$ and spread $\hat{\sigma}_\theta$ values shown in Figure 2 are both normalized by the offshore array values and thus provide an indication of the fraction of energy lost through breaking seaward of the observation location and the associated directional broadening of the wave spectrum. When $\hat{F}_x > 0.7$, i.e., observations on the outer edge or seaward of the surf zone, $\hat{\sigma}_\theta$ generally varies between 0.5 and 0.9, indicating refractive nar-

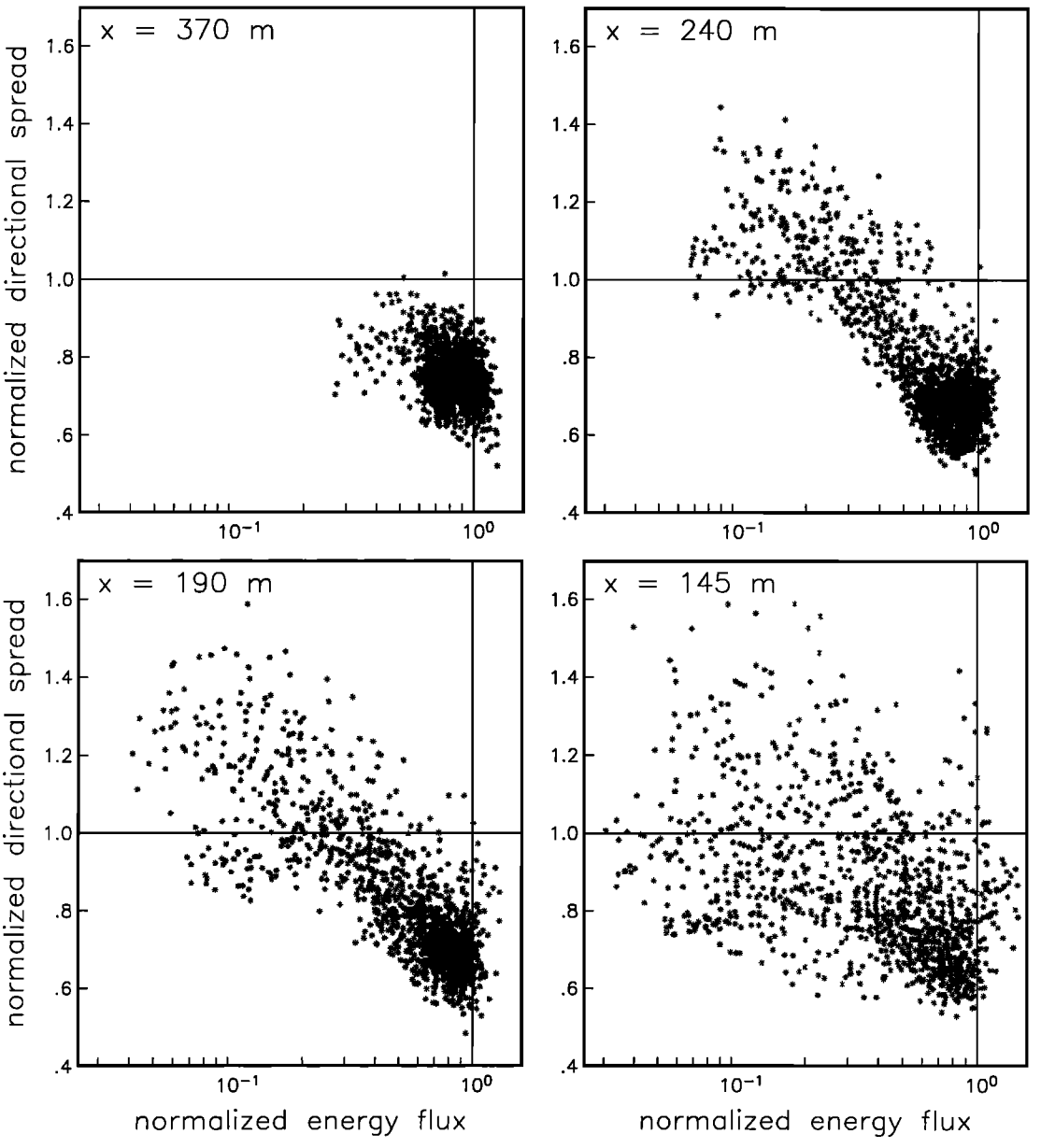

Figure 2. Frequency-integrated directional spread versus cross-shore energy flux (both normalized by the offshore x = 900 m values) at cross-shore positions x = 370 m (seaward of the bar crest), 240 m (on the bar crest), 190 m (slightly inshore of the bar crest), and 145 m (at the toe of the beach face). Each asterisk represents an estimate based on a 1-hour-long data record.

rowing of the wave field. In contrast, directional broadening is evident for $\hat{F}_x < 0.3$ observations well inside the surf zone, with $\hat{\sigma}_\theta$ typically ranging from 0.9–1.4. A trend of increasing directional spread with decreasing energy flux is clearest in the vicinity of the sand bar crest (x = 190 and 240 m) but is also observed with more scatter at x = 370 m (usually outside the surf zone) and x = 145 m (often well inside the surf zone).

Differences in the cross-shore evolution of directional spreads with nonbreaking and breaking wave conditions on the sand bar are illustrated in Figure 3a. Breaking conditions are characterized here by the observed normalized energy flux $\hat{F}_x$ at x = 205 m just inshore of the crest of the sand bar. When $\hat{F}_{x,205\mathrm{m}} > 0.7$, waves propagate over the bar with little or no breaking and intense breaking usually does not occur until near the beach face. In these cases the mean value of $\hat{\sigma}_\theta$ estimates decreases gradually from 0.8 at x = 480 m to 0.7 at x = 160 m near the toe of the beach face, followed by an increase to 0.8 at the most shoreward site, which is usually within the surf zone. When $\hat{F}_{x,205\mathrm{m}} < 0.3$, energy losses due to wave breaking on the bar are large and the mean value of $\hat{\sigma}_\theta$ estimates increases over the bar to a maximum value of 1.1 at x = 190–240 m, decreasing to 0.9 near the shoreline. The standard deviations of the $\hat{\sigma}_\theta$ estimates are smaller than the differences between mean values in nonbreaking and breaking conditions.

The velocity measurements (upon which the σ_θ estimates are based) may contain nongravity wave motions such as wave-breaking-induced turbulence. The ratio R between pressure and velocity fluctuations, integrated over the swell-sea frequency range and normalized by the linear theory transfer function

$$R \equiv \left\{ \frac{\int_{0.05\text{Hz}}^{0.25\text{Hz}} df C_{pp}(f)}{\int_{0.05\text{Hz}}^{0.25\text{Hz}} df \left(\frac{2\pi f}{gk}\right)^2 [C_{uu}(f) + C_{vv}(f)]} \right\}^{1/2} \quad (9)$$

is theoretically equal to 1 for gravity waves. For both nonbreaking and breaking wave conditions the mean value ±1 standard deviation of the R estimates fall within the range 0.82–1.14 (Figure 3b). These small [$O(10\%)$] deviations from 1 are comparable with expected uncertainties in the flowmeter response [*Guza et al.*, 1988] and slight nonlinear deviations of the wavenumber k from the dispersion relationship [e.g., *Freilich and Guza*, 1984] not accounted for in (9). Estimates of velocity-pressure transfer functions at individual frequencies (not shown) are similar to the bulk values shown in Figure 3b. The estimated R do not deviate notably from 1 on the bar crest in breaking wave conditions where a large increase in directional spread is observed (Figure 3a), confirming that the observed directionally broad motions are dominated by gravity waves.

4. Frequency Dependence

The frequency dependence of the directional properties $\theta_{\text{mean}}(f)$ and $\sigma_\theta(f)$ observed well seaward of the bar crest at x = 480 m and slightly inshore of the crest at x = 205 m are shown in Figure 4 for the same three example cases as in Figure 1. At x = 480 m the $\sigma_\theta(f)$ estimates for all three cases have a minimum value near the spectral peak frequency f_p (Figures 4g–4i), similar to observations of the directional spreading of wind waves in deep water [e.g., *Mitsuyasu et al.*, 1975; *Hasselmann et al.*, 1980]. On September 27 the nonlinear transformation of normally incident, nonbreaking waves (f_p = 0.1 Hz) over the bar results in a pronounced harmonic peak ($2f_p$ = 0.2 Hz) at x = 205 m (Figure 4a) with mean direction and spread approximately equal to that of the primary peak (f_p), consistent with the theoretical interaction rule (3). On September 30, higher-frequency waves (f_p = 0.2 Hz) are partially dissipated on the sand bar (Figure 4b). These presumably locally generated seas are directionally narrow at x = 480 m [$\sigma_\theta(f_p) = 6°$, Figure 4h] owing to the strong refractive collimation of waves arriving at large oblique angles [$\theta_{\text{mean}}(f_p) = 30°$, Figure 4e; see (10a) and (10b), discussed below]. Wave breaking on the sand bar is accompanied by strong directional broadening of the entire spectrum, nearly doubling σ_θ at all frequencies, including the weak residual 0.1-Hz swell peak (Figure 4h). On October 12, energetic, normally incident seas (f_p = 0.13 Hz) were attenuated strongly by wave breaking over the bar (Figure 4c). Whereas $\theta_{\text{mean}}(f)$ changes little between x = 480 and 205 m (Figure 4f), $\sigma_\theta(f)$ increases, especially near the spectral peak frequency. Breaking and nonlinear interactions apparently have produced a wave field with nearly uniform (over a wide frequency range) energy levels and directional spreading.

For directionally narrow spectra on a beach with straight and parallel depth contours, the shoaling transformation of θ_{mean} and σ_θ between two cross-shore locations x_d and x is given approximately by Snell's law [e.g., *Kinsman*, 1965]

$$\sin [\theta_{\text{mean},x}(f)] = \frac{c_x(f)}{c_{x_d}(f)} \sin [\theta_{\text{mean},x_d}(f)] \quad (10a)$$

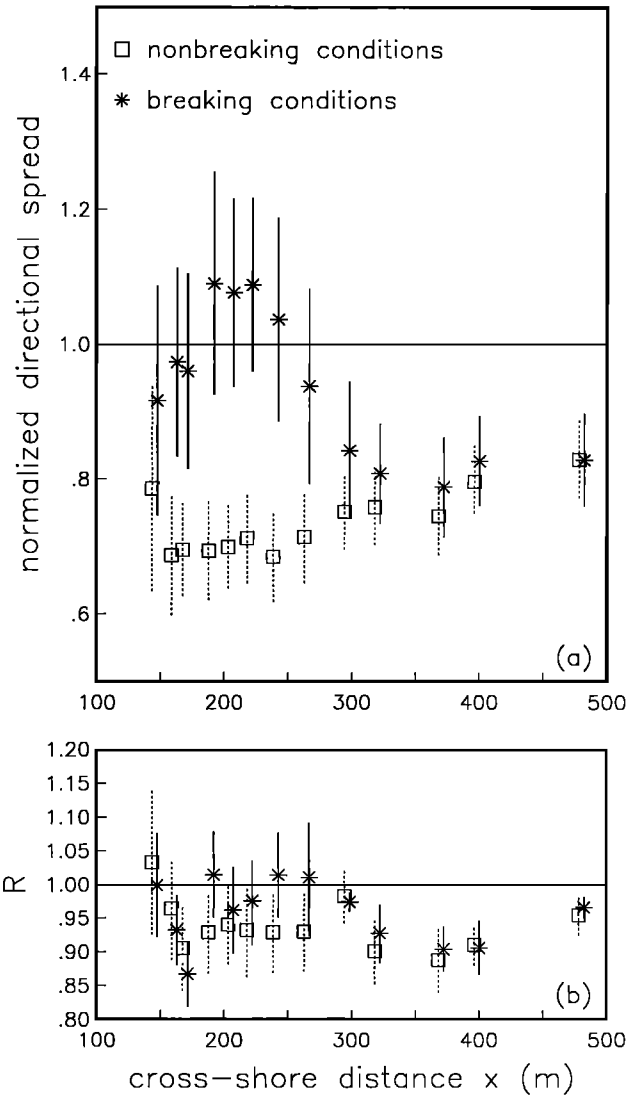

Figure 3. (a) Frequency-integrated directional spread (normalized by the offshore array value) versus cross-shore distance x. Squares represent estimates from 551 one-hour-long data records collected in low-energy wave conditions with small energy losses on the sand bar ($\hat{F}_x > 0.7$ at x = 205 m). Asterisks represent estimates from 304 data records collected in high-energy wave conditions with intense breaking on the sand bar ($\hat{F}_x < 0.3$ at x = 205 m). Symbols and bars indicate the average value ±1 standard deviation of the estimates. (b) Estimated ratio R between pressure and velocity fluctuations, normalized by the theoretical transfer function for linear waves (equation (9)), versus cross-shore distance x (same format as Figure 3a).

$$\sigma_{\theta,x}(f) = \frac{c_x(f)}{c_{x_d}(f)} \frac{\cos [\theta_{\text{mean},x_d}(f)]}{\cos [\theta_{\text{mean},x}(f)]} \sigma_{\theta,x_d}(f) \quad (10b)$$

where c_x denotes the wave phase speed at cross-shore location x. Predictions of $\theta_{\text{mean},x}$ and $\sigma_{\theta,x}$ at the spectral peak frequency f_p were obtained at all instrument locations by substituting the estimates from the offshore array (x_d = 900 m) in (10a) and (10b). Comparisons with observed values are shown in Figure 5 for both nonbreaking and breaking conditions over the bar (using the same energy loss criteria $\hat{F}_{x,205\text{m}} > 0.7$ and <0.3, respectively, as in Figure 3). Predictions of $\theta_{\text{mean},x}(f_p)$

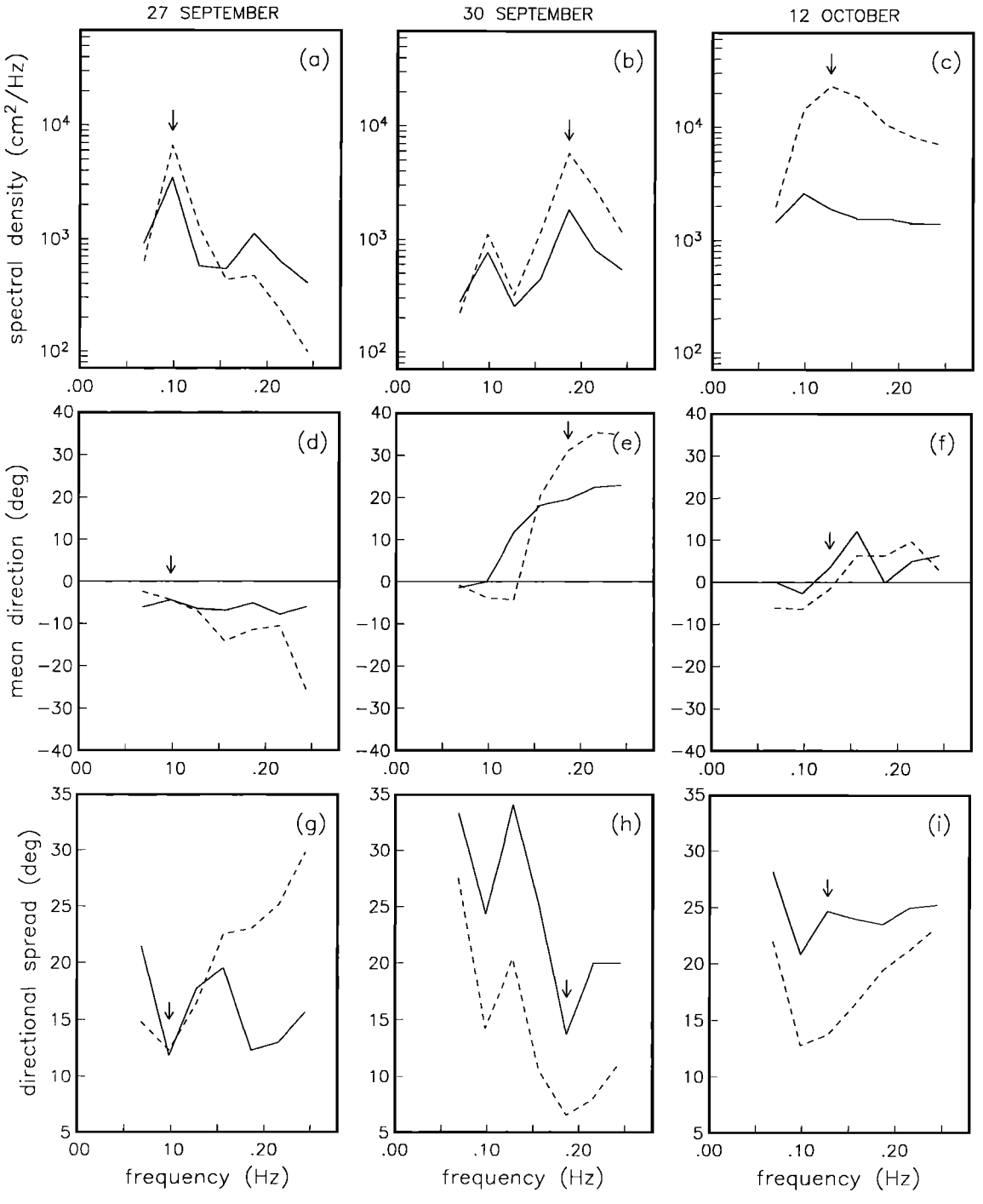

Figure 4. Observed (a–c) spectrum $E(f)$, (d–f) mean propagation direction $\theta_{mean}(f)$, and (g–i) directional spread $\sigma_\theta(f)$ versus frequency for the three case studies shown in Figure 1. Dashed and solid curves indicate estimates well offshore of the bar crest (at x = 480 m in about 5 m depth) and slightly inshore of the bar crest (at x = 205 m in about 2–2.5 m depth), respectively. The spectral peak frequency f_p is indicated with an arrow.

agree well with observations at all locations for both low- and high-energy wave conditions (Figure 5a), indicating that mean propagation directions at the spectral peak frequency are not affected strongly by wave breaking, even in the inner surf zone, where most of the wave energy is dissipated. The corresponding observed and predicted $\sigma_{\theta,x}(f_p)$ (Figure 5b) are also in good agreement for $x > 350$ m, usually offshore of the surf zone. In nonbreaking conditions the directional spreads observed closer to shore are slightly larger than the predicted values. In contrast, the directional spreads observed on and inshore of the bar crest in breaking conditions are a factor of 2–2.5 larger than the predicted values. The close agreement of observed with predicted θ_{mean}, despite these large differences between observed and predicted σ_θ, suggests that the scattering of wave energy into oblique angles induced by wave breaking is roughly symmetric with respect to the mean propagation direction.

The cross-shore evolution of $\theta_{mean}(2f_p)$, the mean direction

of waves with the harmonic frequency twice that of the spectral peak (f_p), is shown in Figure 6. Observed $\theta_{mean}(2f_p)$ in a 0.06-Hz bandwidth are compared with a linear theory prediction based on Snell's law [equation (10a) initialized at the offshore array] and with the observed direction at the peak frequency $\theta_{mean}(f_p)$. In nonbreaking conditions (Figure 6a) the observed $2f_p$ directions diverge slightly from the Snell's law prediction during shoaling (solid curve) but become more closely aligned with the f_p direction (dashed curve). This evolution shows the expected transition of motions at frequency $2f_p$ from free locally generated seas at the offshore array (with directions unrelated to the directions of the lower-frequency swell) to nonlinearly forced harmonic waves at shallower locations [with directions aligned with the primary f_p waves; (3)]. In breaking conditions (Figure 6b) the mean directions of $2f_p$ waves observed at all instrument locations are more closely aligned with waves with frequency f_p (dashed curve) than with the Snell's law prediction (solid curve), suggesting that directionality at harmonic frequencies is governed by nonlinearity along the entire transect.

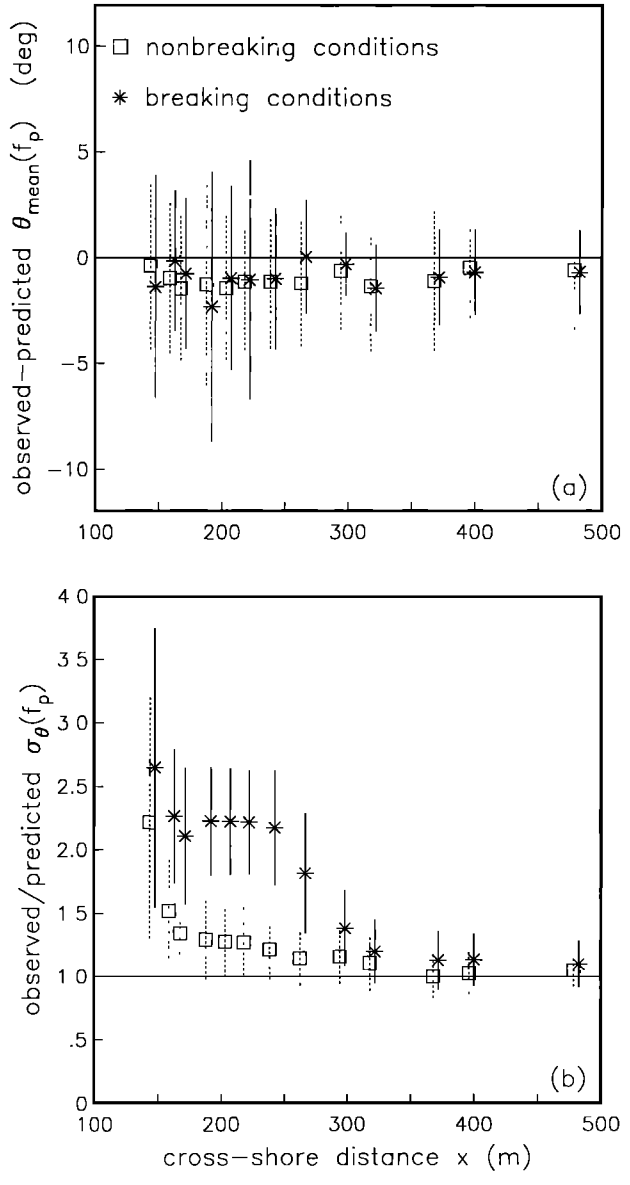

Figure 5. Comparison of observed with predicted (based on Snell's law) directional properties at the spectral peak frequency f_p versus cross-shore distance. (a) Average value and standard deviation of the difference between observed and predicted $\theta_{mean}(f_p)$. (b) Average value and standard deviation of the ratio between observed and predicted $\sigma_\theta(f_p)$. Squares and asterisks represent results for nonbreaking and breaking conditions on the bar, respectively (same format as Figure 3).

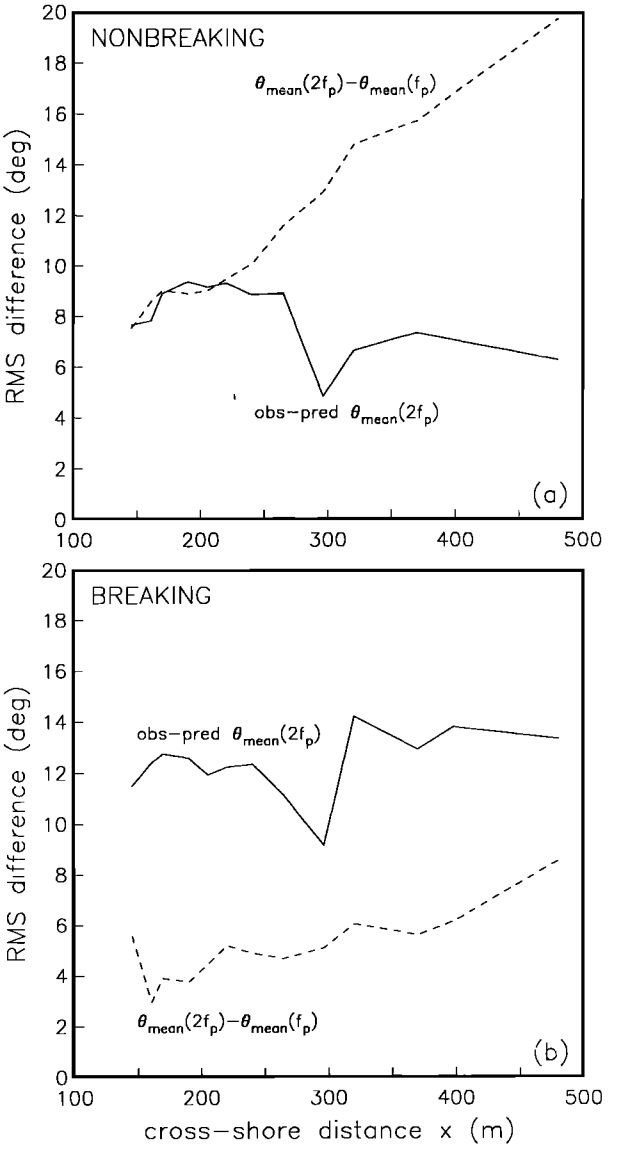

Figure 6. Root-mean-square differences between observed and predicted (based on Snell's law) mean directions of waves with frequency $2f_p$ (solid curves) and between observed $2f_p$ directions and observed f_p directions (dashed curves) versus cross-shore distance for (a) 247 low-energy data records with nonbreaking conditions on the bar and (b) 136 high-energy records with breaking conditions on the bar (using the same energy loss criteria as in Figure 3). Only data records with $2f_p < 0.25$ Hz are included.

Directional spreads observed in breaking wave conditions at the peak frequency $[\sigma_\theta(f_p)]$ and twice the peak frequency $[\sigma_\theta(2f_p)]$ are compared in Figure 7. Offshore of the bar crest ($x > 250$ m), spreads observed at $2f_p$ are about 20–80% larger than the spreads observed at f_p. Shoreward of the bar crest, these differences decrease, and at the shallowest sites the

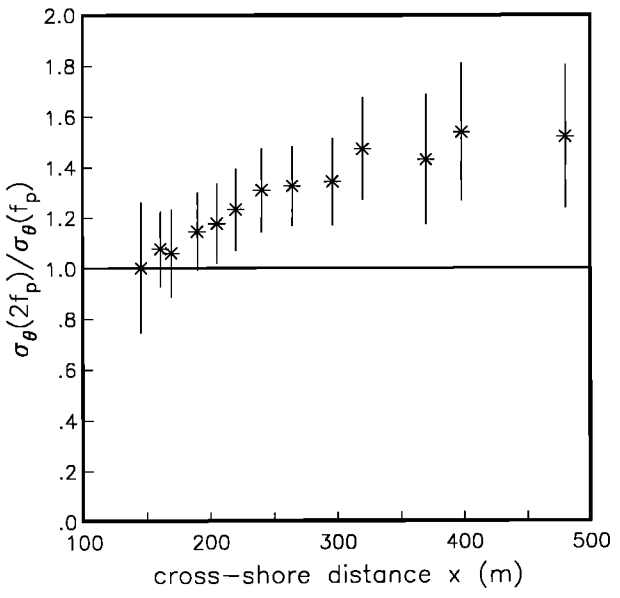

Figure 7. Ratio of directional spreads at frequencies $2f_p$ and f_p observed in high-energy wave conditions with breaking on the bar. Average values ±1 standard deviation (based on 136 observations) are shown versus cross-shore distance.

f_p and $2f_p$ spreads differ by less than ±20%. The corresponding mean directions at frequencies f_p and $2f_p$ converge in a similar fashion (dashed curve in Figure 6b) and differ by less than a few degrees at the shallowest instrument locations.

5. Discussion

To investigate if the barred beach topography plays a critical role in the observed directional broadening of waves in the surf zone, observations from collocated pressure sensors and bidirectional current meters obtained at nonbarred Torrey Pines Beach, near La Jolla, California, were analyzed. Data were collected at six locations along a cross-shore transect extending from the shoreline to about 4 m depth (Figure 8a), with a sample frequency of 2 Hz between September 13 and October 25, 1996 (B. Raubenheimer et al., Tidal water table fluctuations in a sandy ocean beach, submitted to *Water Resources Research*, 1998). Two examples of the cross-shore evolution of frequency-integrated directional spreads [equation (7b)] are shown in Figure 8 for a high- and a low-tide data record with nearly identical incident wave conditions (normally incident swell with a significant wave height of 0.8 m and a peak frequency of 0.08 Hz). Frequency-integrated mean direction estimates (not shown) from all sensors vary between −3° and 10°. During the high-tide run, σ_θ decreases slightly between the deepest sensor and the outer edge of the surf zone ($x \approx 200$ m), followed by an increase (about a factor 2) to a maximum at the shallowest sensor. During low tide, when more instruments were in the surf zone, σ_θ increases gradually along the entire transect to a maximum near the shoreline that is a factor 3 larger than the offshore estimate.

Comparison of all directional spread estimates at $x = 206$ m (in the middle of the transect) and $x = 126$ m (the shallowest sensor) with the local energy flux (Figure 9) demonstrates a clear correspondence between surf zone wave breaking and increased directional spreading. Although these nonbarred beach observations span a more limited range of wave conditions than the barred beach observations, the similar results (compare Figure 9 with Figure 2) indicate that the increased directional spreading initiated by wave breaking is not extremely sensitive to the detailed beach topography. The barred beach observations show maximum directional spreading near the crest of the sand bar (Figures 1d and 3a), and the nonbarred beach observations show maximum directional spreading near the shoreline (Figure 8c). This difference may be the result of different wave-breaking patterns. After breaking on a sand bar, waves may reform in the slightly deeper trough shoreward of the sand bar [*Lippmann and Holman*, 1990]. In contrast, once breaking begins on a monotonically sloping beach, strong dissipation continues until the shoreline.

Although the present results indicate a significant broadening of the directional wave spectrum in the surf zone, the cause of this phenomenon is not understood. A possible mechanism for scattering wave energy into oblique propagation directions is nonlinear triad interactions. During the initial shoaling evolution of the wave spectrum, energy is transferred primarily through sum interactions to higher frequencies. Two components with frequencies and directions (f_1, θ_1) and (f_2, θ_2) transfer energy to a sum-frequency ($f_3 = f_1 + f_2$) wave with a propagation direction θ_3 that falls within the range [θ_1, θ_2] and thus does not directionally broaden the wave field. During breaking the strongly enhanced high-frequency components of the spectrum may transfer some energy back to lower frequencies through difference interactions. According to the interaction rules [see (1)–(3)], two components with frequencies and directions (f_2, θ_2) and (f_3, θ_3) can transfer energy to a difference-frequency ($f_1 = f_3 - f_2$) component with a propagation direction

$$\theta_1 = \frac{f_3}{f_3 - f_2}\theta_3 - \frac{f_2}{f_3 - f_2}\theta_2 \tag{11}$$

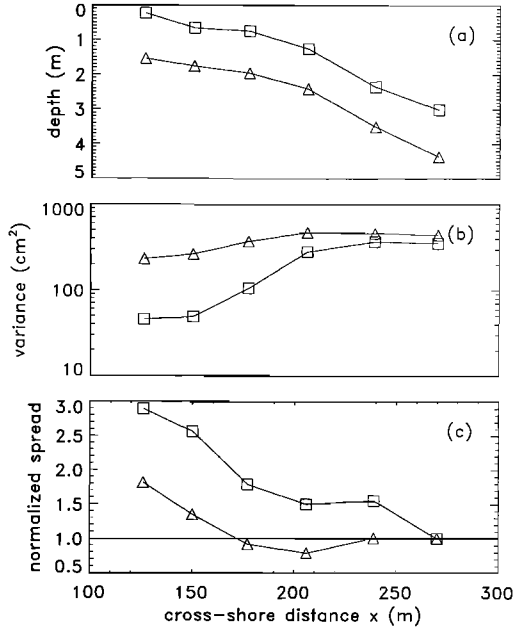

Figure 8. (a) Water depth, (b) sea surface height variance, and (c) frequency-integrated directional spread versus cross-shore distance at Torrey Pines Beach on September 29 (triangles, high tide) and September 30 (squares, low tide), 1996. Data records are approximately 3 hours long.

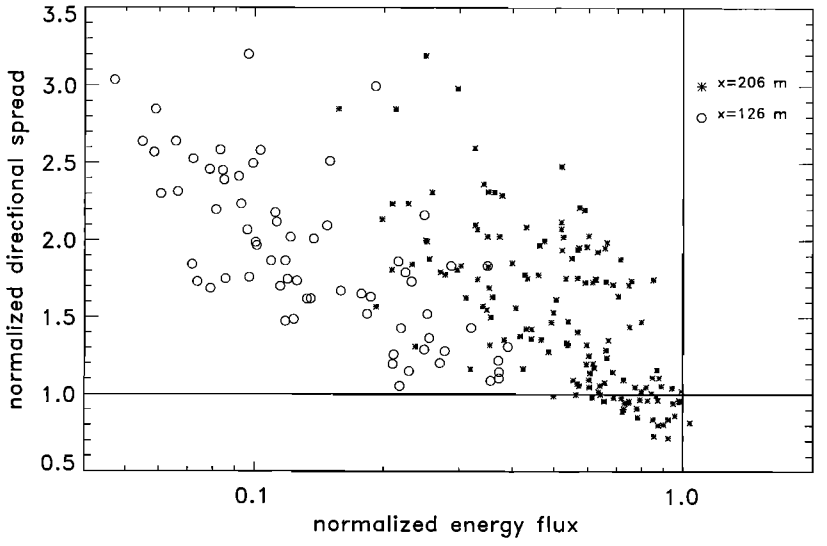

Figure 9. Frequency-integrated directional spread versus cross-shore energy flux (both normalized by estimates from the most offshore instrument) observed at Torrey Pines Beach. Estimates are based on 3-hour-long records from instruments at cross-shore positions x = 206 m (asterisks) and 126 m (circles).

that is outside the range $[\theta_2, \theta_3]$ and thus causes a directional broadening of the wave field. For example, consider the simple case of two incident swell components with the same frequency f and slightly different incidence angles $\theta - \Delta\theta$ and $\theta + \Delta\theta$. Sum interactions [equations (2a) and (3)] excite three double-frequency ($2f$) components with directions $\theta - \Delta\theta$, θ, and $\theta + \Delta\theta$. Subsequent difference interactions [equations (2a) and (11)] between the new $2f$ and the original f components not only transfer energy back to the two original f components but also excite two new f components (f, $\theta - 3\Delta\theta$) and (f, $\theta + 3\Delta\theta$) with a larger spreading angle. Further interactions that involve these newly formed waves may transfer energy to even larger spreading angles. Although the effectiveness of this mechanism has not been established, multiple triad interactions potentially can scatter energy from directionally narrow incident waves into obliquely propagating components.

6. Summary

Mean wave propagation directions at the spectral peak frequency f_p observed both inside and outside the surf zone on a barred beach agree well with predictions based on Snell's law for wave refraction over straight and parallel depth contours (Figure 5a). During shoaling, mean directions of waves with frequency $2f_p$ become aligned closely with the directions of the dominant f_p waves (Figure 6a), consistent with the theoretical interaction rules for nonlinear energy transfers to harmonic components. Whereas mean directions do not appear to be affected strongly by the onset of wave breaking on the sand bar, the corresponding directional spread of wave energy about the mean direction increases dramatically when waves break over the bar (Figures 1d, 2, 3a, and 5b). Well inside the surf zone, the observed mean direction and directional spread are nearly independent of frequency (Figures 4i, 6b, and 7).

Observations of wave shoaling on a nonbarred beach (Figures 8 and 9) show a similar increase in directional spreading in the surf zone, suggesting that the broadening is primarily the result of wave breaking and is not sensitive to the detailed beach topography. The scattering process is not understood well, and more detailed observations are needed to resolve the directional wave properties (e.g., contributions of edge waves). The observed increases of directional spreads in the surf zone are large (nominally a factor of 2) and may have important implications for the dynamics of nearshore wave-driven currents.

Appendix: Estimation of Directional Moments

The cross spectra of a collocated pressure sensor and bidirectional current meter yield low-resolution directional wave information equivalent to that obtained from measurements of commonly used surface-following heave-pitch-roll buoys [*Longuet-Higgins et al.*, 1963; *Bowden and White*, 1966; *Long*, 1980]. The normalized cospectra of pressure p, and the horizontal (x, y) velocity components u and v yield the lowest four Fourier moments of the directional distribution of wave energy $S(\theta)$ [$\equiv E(f, \theta)/E(f)$]

$$a_1(f) \equiv \int_{-\pi}^{\pi} d\theta \cos \theta S(\theta; f) = \frac{C_{pu}(f)}{\{C_{pp}(f)[C_{uu}(f) + C_{vv}(f)]\}^{1/2}} \quad \text{(A1a)}$$

$$b_1(f) \equiv \int_{-\pi}^{\pi} d\theta \sin \theta S(\theta; f) = \frac{C_{pv}(f)}{\{C_{pp}(f)[C_{uu}(f) + C_{vv}(f)]\}^{1/2}} \quad \text{(A1b)}$$

$$a_2(f) \equiv \int_{-\pi}^{\pi} d\theta \cos 2\theta S(\theta; f) = \frac{C_{uu}(f) - C_{vv}(f)}{C_{uu}(f) + C_{vv}(f)} \quad \text{(A1c)}$$

$$b_2(f) \equiv \int_{-\pi}^{\pi} d\theta \sin 2\theta S(\theta; f) = \frac{2C_{uv}(f)}{C_{uu}(f) + C_{vv}(f)} \quad \text{(A1d)}$$

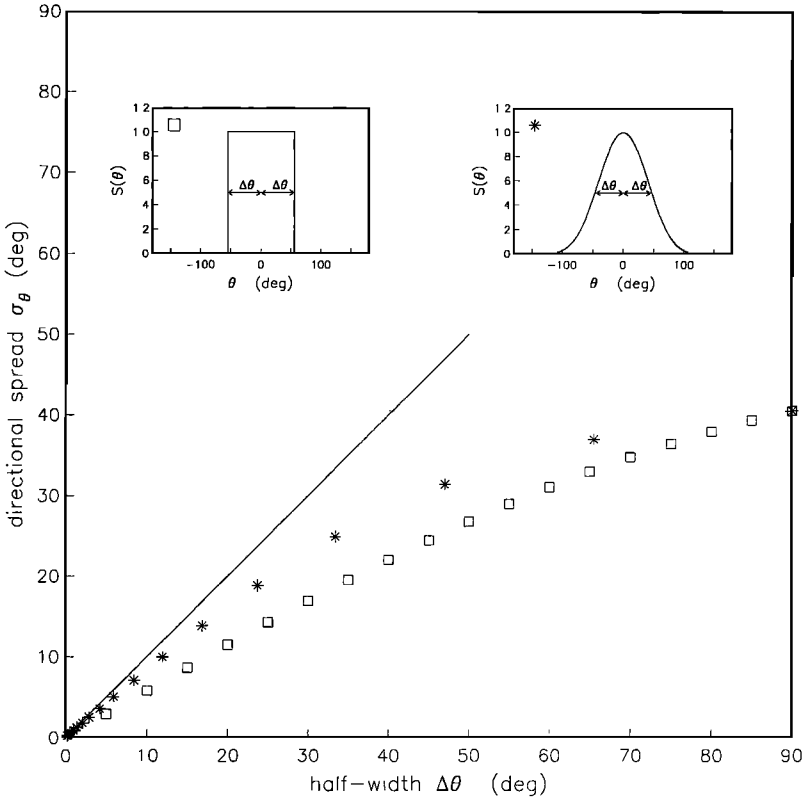

Figure A1. Directional spread σ_θ versus the half width $\Delta\theta$ of the directional distribution $S(\theta)$ at half the maximum power, for top-hat (squares) and cosine-power (asterisks) shapes of $S(\theta)$. The solid line denotes a 1:1 correspondence, and the dotted line indicates the maximum value of σ_θ for a directionally isotropic wave–orbital velocity field.

where $\theta = 0$ corresponds to onshore propagation. Note that estimates of these directional moments are insensitive to instrument gain errors, so long as the errors are the same on both flowmeter axes.

For narrow $S(\theta)$, a mean propagation direction θ_{mean} and a root-mean-square measure of the directional spreading of wave energy σ_θ can be defined in terms of the first-order moments a_1 and b_1 [e.g., *Kuik et al.*, 1988]

$$\int_{-\pi}^{\pi} d\theta \sin(\theta - \theta_{\text{mean}})S(\theta) = b_1 \cos\theta_{\text{mean}} - a_1 \sin\theta_{\text{mean}} = 0 \tag{A2a}$$

$$\sigma_\theta^2 \equiv \int_{-\pi}^{\pi} d\theta 2[1 - \cos(\theta - \theta_{\text{mean}})]S(\theta)$$

$$= 2[1 - (a_1 \cos\theta_{\text{mean}} + b_1 \sin\theta_{\text{mean}})] \tag{A2b}$$

For small $\theta - \theta_{\text{mean}}$

$$\sin(\theta - \theta_{\text{mean}}) \approx (\theta - \theta_{\text{mean}})[1 - \tfrac{1}{6}(\theta - \theta_{\text{mean}})^2]$$

$$2[1 - \cos(\theta - \theta_{\text{mean}})] \approx (\theta - \theta_{\text{mean}})^2[1 - \tfrac{1}{12}(\theta - \theta_{\text{mean}})^2]$$

and thus θ_{mean} and σ_θ represent a mean value and standard deviation of the directional distribution of wave energy with an $O(\theta - \theta_{\text{mean}})^2$ bias (see *Kuik et al.* [1988] for further discussion).

A serious drawback of this formulation is the sensitivity of σ_θ to reflection of waves from shore. Although most of the incident wave energy usually is dissipated in the surf zone, significant reflection from shore may occur if the incident waves are small in amplitude and the beach is relatively steep [*Miche*, 1951]. Measurements of wave reflection from natural sandy beaches [*Elgar et al.*, 1994, 1997; *Raubenheimer and Guza*, 1996] show a strong frequency dependence, with reflection levels that are barely detectable (less than 3% of the total wave energy) at sea frequencies (>0.1 Hz), often significant [$O(10\%)$] at swell frequencies (0.05–0.1 Hz) and consistently strong at infragravity frequencies (<0.05 Hz). Whereas σ_θ is equal to zero for unidirectional waves, σ_θ is increased to 36° by a directionally opposing component with only 10% of the total wave energy [equation (A2b)]. Thus weak reflection from shore may be misinterpreted as a directionally broad incident wave field.

Alternatively, θ_{mean} and σ_θ can be defined in terms of the second-order moments a_2 and b_2:

$$\int_{-\pi}^{\pi} d\theta \tfrac{1}{2} \sin[2(\theta - \theta_{\text{mean}})]S(\theta)$$

$$= \tfrac{1}{2}(b_2 \cos 2\theta_{\text{mean}} - a_2 \sin 2\theta_{\text{mean}}) = 0 \tag{A3a}$$

$$\sigma_\theta^2 \equiv \int_{-\pi}^{\pi} d\theta \tfrac{1}{2}\{[1 - \cos[2(\theta - \theta_{\text{mean}})]\}S(\theta)$$

$$= \tfrac{1}{2}[1 - (a_2 \cos 2\theta_{\text{mean}} + b_2 \sin 2\theta_{\text{mean}})] \tag{A3b}$$

For small $\theta - \theta_{\text{mean}}$

$$\tfrac{1}{2}\sin[2(\theta - \theta_{\text{mean}})] \approx (\theta - \theta_{\text{mean}})[1 - \tfrac{2}{3}(\theta - \theta_{\text{mean}})^2]$$

$$\tfrac{1}{2}\{1 - \cos[2(\theta - \theta_{\text{mean}})]\} \approx (\theta - \theta_{\text{mean}})^2[1 - \tfrac{1}{3}(\theta - \theta_{\text{mean}})^2]$$

and thus the second-order approximations (A3a) and (A3b) of the mean value and standard deviation of $S(\theta)$ have larger biases than the first-order approximations (A2a) and (A2b). However, (A3a) and (A3b) are much less sensitive than (A2a) and (A2b) to wave reflections from shore at small incidence angles because the double-angle argument $2(\theta - \theta_{\text{mean}})$ is the same for waves propagating in opposing directions.

The interpretation of σ_θ estimates based on (A3b) is illustrated in Figure A1 with simple cosine-power and top-hat $S(\theta)$ functions. For both distributions, σ_θ is roughly comparable with the half width $\Delta\theta$ with a negative bias that increases with increasing $\Delta\theta$. The maximum σ_θ value of 40.5° for $\Delta\theta = 90°$ corresponds to wave motion with an isotropic velocity field ($C_{v'v'} = C_{u'u'}$).

Acknowledgments. This research was supported by the Coastal Dynamics Program of the Office of Naval Research and the Ocean Sciences Division of the National Science Foundation (Coastal Ocean Processes program). The instruments were deployed and maintained by staff from the Scripps Institution of Oceanography Center for Coastal Studies. B. Raubenheimer and E. L. Gallagher made valuable contributions to the field experiments. Logistical support and wave data in 8 m depth were provided by the Field Research Facility of the U.S. Army Engineer Waterways Experiment Station's Coastal Engineering Research Center. Permission to use these data is appreciated.

References

Battjes, J. A., Radiation stresses in short-crested waves, *J. Mar. Res.*, *30*, 56–64, 1972.

Bowden, K. F., and R. A. White, Measurements of the orbital velocities of sea waves and their use in determining the directional spectrum, *Geophys. J. R. Astron. Soc.*, *12*, 33–54, 1966.

Bryan, K. R., and A. J. Bowen, Edge wave trapping and amplification on barred beaches, *J. Geophys. Res.*, *101*, 6543–6552, 1996.

Elgar, S., R. T. Guza, and M. H. Freilich, Observations of nonlinear interactions in directionally spread shoaling surface gravity waves, *J. Geophys. Res.*, *98*, 20,299–20,305, 1993.

Elgar, S., T. H. C. Herbers, and R. T. Guza, Reflection of ocean surface gravity waves from a natural beach, *J. Phys. Oceanogr.*, *24*, 1503–1511, 1994.

Elgar, S., R. T. Guza, B. Raubenheimer, T. H. C. Herbers, and E. L. Gallagher, Spectral evolution of shoaling and breaking waves on a barred beach, *J. Geophys. Res.*, *102*, 15,797–15,805, 1997.

Freilich, M. H., and R. T. Guza, Nonlinear effects on shoaling surface gravity waves, *Philos. Trans. R. Soc. London, Ser. A*, *A311*, 1–41, 1984.

Freilich, M. H., R. T. Guza, and S. Elgar, Observations of nonlinear effects in directional spectra of shoaling gravity waves, *J. Geophys. Res.*, *95*, 9645–9656, 1990.

Gallagher, E. L., S. Elgar, and R. T. Guza, Observations of sand bar evolution on a natural beach, *J. Geophys. Res.*, *103*, 3203–3215, 1998.

Guza, R. T., and E. B. Thornton, Velocity moments in nearshore, *J. Waterw. Port Coastal Ocean Eng.*, *111*, 235–256, 1985.

Guza, R. T., M. C. Clifton, and F. Rezvani, Field intercomparisons of electromagnetic current meters, *J. Geophys. Res.*, *93*, 9302–9314, 1988.

Hasselmann, D. E., M. Dunckel, and J. A. Ewing, Directional wave spectra observed during JONSWAP 1973, *J. Phys. Oceanogr.*, *10*, 1264–1280, 1980.

Herbers, T. H. C., and M. C. Burton, Nonlinear shoaling of directionally spread waves on a beach, *J. Geophys. Res.*, *102*, 21,101–21,114, 1997.

Higgins, A. L., R. J. Seymour, and S. S. Pawka, A compact representation of ocean wave directionality, *Appl. Ocean Res.*, *3*, 105–112, 1981.

Kinsman, B., *Wind Waves: Their Generation and Propagation on the Ocean Surface*, 676 pp., Prentice-Hall, Englewood Cliffs, N. J., 1965.

Kuik, A. J., G. P. van Vledder, and L. H. Holthuijsen, A method for routine analysis of pitch-and-roll buoy data, *J. Phys. Oceanogr.*, *18*, 1020–1034, 1988.

Lippmann, T. C., and R. A. Holman, The spatial and temporal variability of sand bar morphology, *J. Geophys. Res.*, *95*, 11,575–11,590, 1990.

Lippmann, T. C., and R. A. Holman, Phase speed and angle of breaking waves measured with video techniques, in *Coastal Sediments '91*, pp. 542–556, Am. Soc. Civ. Eng., New York, 1991.

Long, C. E., Index and bulk parameters for frequency-direction spectra measured at CERC Field Research Facility, June 1994 to August 1995, *Misc. Pap. CERC-96-6*, U.S. Army Eng. Waterw. Exp. Stn., Vicksburg, Miss., 1996.

Long, R. B., The statistical evaluation of directional spectrum estimates derived from pitch/roll buoy data, *J. Phys. Oceanogr.*, *10*, 944–952, 1980.

Longuet-Higgins, M. S., D. E. Cartwright, and N. D. Smith, Observations of the directional spectrum of sea waves using the motions of a floating buoy, in *Ocean Wave Spectra*, pp. 111–136, Prentice-Hall, Englewood Cliffs, N. J., 1963.

Miche, M., Le pouvoir reflechissant des ouvrages maritimes exposes a l'action de la houle, *Ann. Ponts Chaussees*, *121*, 285–319, 1951.

Mitsuyasu, H., F. Tasai, T. Suhara, S. Mizuno, M. Ohkusu, T. Honda, and K. Rikiishi, Observations of the directional spectrum of ocean waves using a cloverleaf buoy, *J. Phys. Oceanogr.*, *5*, 750–760, 1975.

Raubenheimer, B., and R. T. Guza, Observations and predictions of run-up, *J. Geophys. Res.*, *101*, 25,575–25,587, 1996.

S. Elgar, School of Electrical Engineering and Computer Science, Washington State University, Pullman, WA 99164-2752.

R. T. Guza, Center for Coastal Studies, Scripps Institution of Oceanography, La Jolla, CA 92093-0209.

T. H. C. Herbers, Department of Oceanography, Naval Postgraduate School, Code OC/He, Monterey, CA 93943-5122. (herbers@oc.nps.navy.mil)

(Received December 9, 1997; accepted May 22, 1998.)